Photochemical & Photobiological Sciences

PAPER

Photo-assisted inactivation of *Escherichia coli* bacteria by silver functionalized titanate nanotubes, $Ag/H_2Ti_2O_5{\cdot}H_2O$

Cite this: DOI: 10.1039/c6pp00237d

A. Patron-Soberano,[a] B. P. Núñez-Luna,[b] S. Casas-Flores,[a] A. De las Peñas,[a] R. B. Domínguez-Espíndola[c] and V. Rodríguez-González *[b]

Received 1st July 2016,
Accepted 7th April 2017

DOI: 10.1039/c6pp00237d

rsc.li/pps

One-dimensional titanate nanotubes ($H_2Ti_2O_5{\cdot}H_2O$) functionalized with silver nanoparticles (AgNPs) exhibited unique properties for the effective inactivation of the Gram-negative *Escherichia coli* within 45 minutes under irradiation using a 65 W halogen lamp. The pathway of the photo-assisted catalytic inactivation was examined by SEM and TEM using a reproducible biological protocol for sample preparations. The membrane integrity of the bacteria was damaged due to the oxidative stress caused by the reactive oxygen species, the bacteriostatic effect of the highly-dispersed-surface AgNPs (~5 nm) and the sharp nanotube penetration that induced the cell death.

Introduction

Escherichia coli (*E. coli*) is a valuable model microorganism to study the persistence, evolution and inactivation of microorganisms in water sources and soil and on common surfaces such as stainless steel, wood, concrete and plastic.[1–3] *E. coli* is a Gram-negative Enterobacter species that is widely distributed in water, food and mammals, where it naturally colonizes the colon, being pathogenic in some cases. Several *E. coli* strains cause diverse intestinal and extraintestinal diseases by means of virulence, which affects a wide range of cellular processes.[1,2] Infections with hazardous *Escherichia coli* strains could happen through farming products and occur often due to manure-contaminated soil and irrigation water. In cities, the infections may be originating from communal surfaces in public transport, supermarkets, schools, and streets, or in public parks from feces of domestic animals, as well as by means of old potable water system networks and by damaged wastewater drain systems, among others that affect public health.[1–3]

Novel friendly nanotechnologies have been developed in order to study the deactivation of pathogenic microorganisms.[4,5] These microorganisms require conducive environmental conditions in order to survive and reproduce, usually 37 °C, humid surfaces, aerobic conditions and food sources like carbohydrates, proteins, and fats.[6] The thermal inactivation of *E. coli* is linked with the irreversible denaturation of membranes, ribosomes, and nucleic acids,[7] and cell membrane rupture of the bacteria through a direct contact killing mechanism has been proposed for the annihilation of *E. coli*.[5] On the other hand, electrochemical reactions have been conducted on the surface of aligned multi-walled carbon nanotubes decorated with AgNPs.[8] In sonoelectrocatalytic disinfection using TiO_2 as the electrode, the direct and indirect oxidations of *E. coli* cells take place on the TiO_2 surface in 60 min.[9] The irradiation of sol–gel TiO_2-N dense films has shown bactericidal activity in 24 h against *E. coli*.[10] The activity was correlated with the irradiation time, which also showed a detrimental effect due to the generated heat. The catalytic and photocatalytic inactivations of pathogenic microorganisms are adequate and promising techniques that can work under these conditions. The use of nanomaterials with high-surface-to-volume ratios and photoactive, hydrophilic and antibacterial properties has been widely explored.[4–15] Titanium dioxide-based nanomaterials have been the most studied for photoactive microorganism inactivation among semiconductor oxides.[4,7–22] The addition of silver or copper nanoparticles enhances the biocidal and bacteriostatic properties for a whole range of pathogenic microorganisms.[12–14,18,19,22] Titanate materials have structural similarities that are close to those of titanium dioxide, but with the advantage of sharp 1D morphologies such as nanofibers, nanowires, nanoribbons and nanotubes.[16,17] The layered nanomaterials ensure high surface-to-volume ratios, structural defects and oxygen

[a]*División de Biología Molecular, Instituto Potosino de Investigación Científica y Tecnología, San Luis Potosí, S. L. P., Mexico*
[b]*División de Materiales Avanzados, Instituto Potosino de Investigación Científica y Tecnología, San Luis Potosí, S. L. P., Mexico. E-mail: vicente.rdz@ipicyt.edu.mx, vicenrg@hotmail.com; Tel: +52448342000, ext: 7295*
[c]*Posgrado de Ingeniería Química Aplicadas. Universidad Autónoma del Estado de Morelos, Mexico*

vacancies that can be positive for the deactivation of harmful microorganisms. Protonated nanotubes are mainly synthesized by hydrothermal processes using TiO_2 as the precursor.[4,16,17] There are some reports on the use of nanotubes or nanotube blocks based on TiO_2 with the incorporation of AgNPs which exhibit a long-term antibacterial ability[4,5,12,18,22–24] to inactivate and prevent the bacterial adhesion of pathogenic microorganisms.

In the present study, the pathway of *E. coli* inactivation by means of silver nanoparticles functionalized on titanate nanotubes, used as photoactive catalysts, is investigated. The damage and killing effects on *E. coli* were observed and evaluated by SEM and TEM. N_2 physisorption, XRD and UV-vis-DRS were used to perform the physicochemical characterization of the AgNP/titanate nanocomposites.

Experimental

Hydrothermal synthesis of $H_2Ti_2O_5{\cdot}H_2O$

$H_2Ti_2O_5{\cdot}H_2O$ nanotubes were synthesized by a practical hydrothermal method in a microwave reactor (Eyela MWO-1000 Wave Magic) by following our earlier procedure.[20] Protonated titanate nanotubes were obtained in only 4 h under a maximal microwave radiation of 180 W at 150 °C. The precipitated materials were neutralized with a 5 M HCl solution. Then, the resulting powders were filtered and dried for 10 h at 80 °C. The obtained powders were referred to as TNs.

Catalysts

Photodeposition of silver nanoparticles was carried out in an ethanolic solution of $AgNO_3$, placing three loads (0.5, 1 and 3 wt%) and 50 mg of either TNs or P25 (commercial TiO_2 from Evonik) in a small glass reactor. The suspension was kept under vigorous stirring for 5 min and then in an ultrasonic bath for 5 min to ensure the complete disaggregation of precursor particles. Afterwards, the slurry was maintained under magnetic stirring for 1 h and, at the same time, irradiated with a 17 W UVC lamp (TecnoLite G15 T8, 254 nm, 1168 W cm^{-2}). Then, the suspension was filtered using a hydrophilic polypropylene filter (Pall, 0.2 μm) in a vacuum system. The solids were completely dried overnight in an oven at 80 °C. The obtained composites were referred to as Ag*X*TNs, where *X* denotes different silver contents in wt%.

The silver functionalized nanotubes (AgTNs) were characterized using a transmission electron microscope (TEM); HRTEM and HAADF images were obtained with a FEI Tecnai F30 microscope equipped with a tungsten field emission gun operated at 300 keV. UV-vis-DRS molecular spectra were obtained using a UV-vis-NIR Agilent Technologies Cary 5000 spectrophotometer equipped with an integration sphere. X-ray diffraction patterns were obtained using a Bruker Discover X-ray diffractometer with Cu Kα radiation of 1.5406 Å, operated at 35 kV and 25 mA. N_2 adsorption–desorption at −196 °C was carried out using a NOVA 3 instrument on previously outgassed samples at 150 °C. The Brunauer–Emmett–Teller method (BET method) was used to calculate the specific surface area.

Escherichia coli

E. coli was grown in LB medium for 24 h at 30 °C. The culture was centrifuged twice at 4500 rpm for 10 min, the supernatant was discarded and bacterial pellets were resuspended in M9 liquid medium and adjusted to a concentration of ~1×10^9 CFU mL^{-1}. This concentration of *Escherichia coli* TOP10F strain was used in all the experiments.

Photocatalytic deactivation of *Escherichia coli*

The photocatalytic deactivation experiment was carried out in 24 well cell culture plates with constant magnetic stirring (350 rpm), which were irradiated with a halogen lamp (Smart halogen 65 W, Panasonic Corporation) to provide visible light radiation in the presence of 1 mg mL^{-1} of photoactive silver-nanotubes. Identical conditions were set in all the experiments related to change the composites in order to test Ag*X*TNs, TNs, P25 or AgNPs at the optimal concentration used for Ag*X*TNs. After each treatment time (5, 15, 30, 45 and 60 min), 0.1 mL was taken for dilution and 0.1 mL was plated on LB. After 24 h of incubation at 30 °C, the colonies at each dilution and each time were visually identified and counted. The photocatalytic deactivation of *E. coli* was expressed as colony forming units per milliliter (CFU mL^{-1}), which is a measure of viable bacterial cells.

Photodegradation of Eosin Y dye

The photocatalytic degradation of Eosin Y dye (LeMont Productos Químicos, indicator grade) was achieved under visible light radiation (Philips Halogen lamp, Halotone UV Block, 50 W). The test was performed in a borosilicate homemade reactor with 250 mL capacity. 20 mg of composites were added into the reactor containing 200 mL of a solution of 10 mg L^{-1} of Eosin Y dye. Before the solution was exposed to visible light radiation, the system was kept in the dark for 60 min in order to achieve the adsorption–desorption equilibrium. The photoactivity degradation rate was recorded by measuring the intensity of the main absorption band of Eosin Y (517 nm) as a function of the irradiation time. At given time intervals, samples were extracted and filtered through a 0.45 μm nylon filter and then monitored with an Agilent Technologies Cary 5000 UV-vis-NIR spectrophotometer.

Morphological characterization of *E. coli*

E. coli was characterized by using SEM. Cell samples were collected at representative time intervals during deactivation. The pellets of bacteria were fixed in 3% glutaraldehyde in sodium phosphate buffer (100 mM) at pH 7.4 and 4 °C for 1 h; the samples were washed four times with the buffer for 15 min each time. Afterwards, the samples were post-fixed with 1% OsO_4 in buffer for 2 h at 4 °C and washed 4 times. The samples were progressively dehydrated with absolute ethanol from 30 to 100% for 10 min at each concentration, and washed twice with 100% absolute ethanol, each washing

lasting 15 min. The critical point drying process was performed in a Tousimis Samdri-PVT-3D, and the dry samples were mounted and gold sputter coated using a Cressington apparatus Model 108 auto and examined using an FEI model Quanta 250 SEM. The SEM was adjusted to 25 kV, spot size 4.5 and WD 10 mm, recording the micrographs using an Everhart Thornley Detector (ETD).

The ultrastructure of *E. coli* was evaluated by TEM. The bacteria were fixed, post-fixed and progressively dehydrated with absolute ethanol until 100% as previously described for the SEM characterization. Then, the pre-inclusion was done in LRW : absolute ethanol 1 : 1 for 2 h and then in pure LRW overnight. The cell pellets were embedded in gelatine capsules and polymerized at 50 °C for 48 h. Ultrathin sections were obtained using a ultramicrotome (RMC) and placed in FCF-100 Cu and contrasted with 2% uranyl acetate for 10 min, followed by 2% lead citrate for 5 min. Finally, the samples were examined using a JEM-200 CX (JEOL) transmission electron microscope operated at 100 kV and equipped with a digital camera (SIA, Germany).

Results and discussion

Physicochemical characterization of $H_2Ti_2O_5{\cdot}H_2O$

The XRD patterns show low-crystallinity materials, and all the reflections can be ascribed to the orthorhombic phase of $H_2Ti_2O_5{\cdot}H_2O$ (JCPDS 47-0124) and the metallic silver crystalline phase (JCPDS 04-0783), Fig. 1A. Titanic acid is the main crystalline phase in the nanocomposites. At low content of silver loads, no reflection peak characteristic of metallic silver was detected, presumably due to the nanometre size of the highly dispersed silver particles. For 3 wt% of AgNPs, two peaks ascribed to metallic silver were observed. The surface specific areas of the nanocomposites were 300 $m^2\ g^{-1}$ and only a loss of 15% of area occurred when 3 wt% of AgNPs were functionalized. The textural characteristics of the materials were those of mesoporous materials with a Type IV adsorption–desorption isotherm, common for layered materials, Fig. 1B. The absorbed N_2 volume decreased slightly when the silver load was increased due to the P/P_0 thin hysteresis range H2 with the thin region from low P/P_0 values (0.2) to high P/P_0 (0.95), according to the IUPAC classification.[16,17,20] The pore size distribution inset in Fig. 1B shows the maximum pore size at 5 nm in an interval ranging from 2 to 10 nm. UV–vis spectra with surface procedures confirmed the presence of AgNPs (~5 nm) on the surface of one-dimensional nanostructures, see Fig. 1C–E, which is appropriate for visible light excitation. The values of the energy band gap (E_g) were calculated using the equation $\alpha(h\nu) = A(h\nu - E_g)^{m/2}$, where α is the absorption coefficient, $h\nu$ is the photon energy, A is a constant and $m = 2$ for a direct transition between the valence band and the conduction band. For the estimation of the E_g from the UV–vis spectra, a straight line was extrapolated from the absorption curve to the abscissa axis. When α is zero, $E_g = h\nu$. The E_g of a silver titanate is 3.35 eV and it is 3.3 eV for Ag3NTs, on average. The surface plasmon resonance of AgNPs enhances the visible light absorption (Fig. 1C). The thickness of the $H_2Ti_2O_5{\cdot}H_2O$ nanotubes was found to be ~10 nm with four layers. Layered nanotubes have a tendency to agglomerate, forming bundles, as can be seen in Fig. 1D–F. The as-synthesized nanotubes presented sharp open-ended structures. The HAADF images show highly dispersed AgNPs all over the titanate surface of the Ag3NTs composite, Fig. 1E. The HRTEM image of the Ag0.5NTs shows an interlayer separation of ~0.73 nm of the titanate nanotube, Fig. 1F.

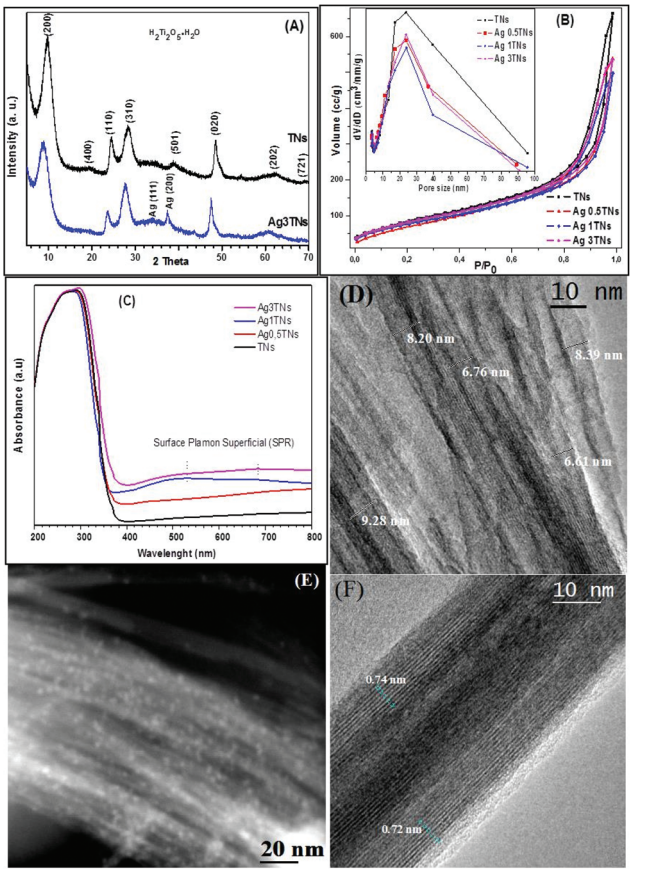

Fig. 1 (A) XRD patterns of TNs and Ag3NTs, (B) adsorption–desorption of N_2 isotherms with internal pore size distribution, (C) UV-vis spectra of Ag*X*TN composites and TNs, (D)–(E) selected HRTEM and HAADF images of the Ag3TN composite and (F) HRTEM image of TNs.

To verify the Ag content in the titanate nanotubes, inductively coupled plasma optical emission spectroscopy (ICP-OES) with a 730-ES spectrometer from Varian Inc. was used. It was determined to be 0.45, 0.92 and 2.45 wt%, respectively.

E. coli deactivation as a function of time by AgNT nanocomposites

The survival of *E. coli* in the plates was evaluated at 5, 15, 30, 45 and 60 min; the CFU mL^{-1} obtained at each time was plotted, obtaining the logarithmic decay of the bacterial growth, Fig. 2. The control test that consists only of *E. coli* colonies as a function of time guarantees the sterilization of the

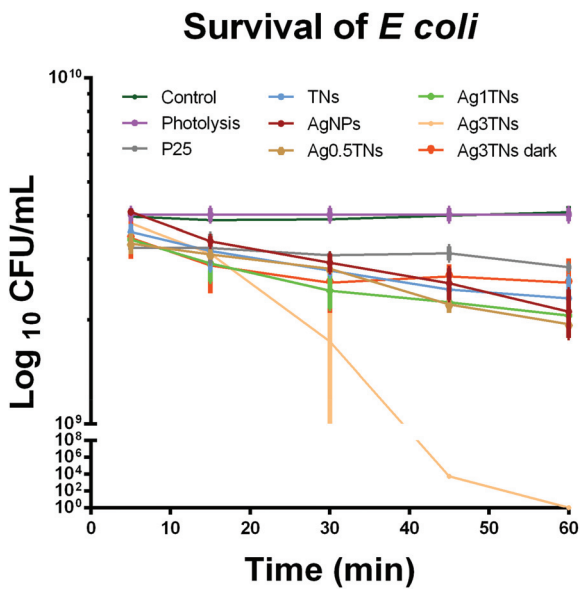

Fig. 2 Logarithmic graph of CFU mL^{-1} *versus* time of *E. coli* after photocatalytic inactivation using Ag*X*TN composites: (A) at different times; (B) behavior at 60 min.

material. The radiation (60 W) without catalyst, identified as photolysis, showed negligible inactivation, suggesting that halogen radiation had no influence on the fatal damage to *E. coli*, Fig. 2.

During the first 30 min of photocatalytic treatment, the photoinactivation was at a very low level in comparison with the control and Ag3TNs under the dark conditions; after 15 min, a strong decrease in the CFU was observed. The complete photoinactivation was achieved at 60 min; thereafter no cell growth in the plate was observed. The treatment with Ag3TNs under dark conditions and the control without treatment did not show viability changes, Fig. 2. In order to clearly show the inactivation differences, the plot shows a magnification of the $\log 10^{-9}$ to $\log 10^{-10}$ interval in a graph of log CFU mL^{-1} from 10^{0} to 10^{-10} that might be overestimated if it were plotted only from 1×10^{-9}. Although the control and photolysis were not affected, a small change was seen in each of the tested nanocomposites; only the Ag3TNs achieved total inactivation after 60 min (Fig. 2). The obtained results are in good agreement with the literature.[4,21–23] The nanocomposites displayed excellent photoactivity and biocidal properties, which is in contrast with the report by Kang *et al.*[24] who, by using an electrode of CdS/Pt-TiO_2 nanotubes, achieved the photoelectro-inactivation of *E. coli* in 60 min. Carbon nanotubes showed biotoxicity against *E. coli* bacteria, achieving a cell loss viability of 80% in 120 min by the oxidative cellular membrane integrity disruption due to the toxicity of single wall carbon nanotubes (SWCNT) and to morphological alteration in 2 h.[5,8]

Morphology and structure of *E. coli* by SEM

Escherichia coli is a Gram-negative, rod-shaped Enterobacter species with dimensions of 1.1–1.5 μm and 2.0–6.0 μm (ref. 25) and belongs to peritrichous bacteria. *Escherichia coli* TOP10F competent cells are smaller with dimensions of 0.1–0.3 μm and 0.7–1.2 μm. Fig. 3A shows control *E. coli* without treatment; the cells show dense straight rod shapes with EPS (Extracellular Polymeric Substances) secretions; Fig. 3B displays *E. coli* exposed to photoinactivation with the Ag3NT sample; the damage to the bacteria is shown by surface undulations, membrane depressions, EPS decreases and increased sizes; although most of the population are dead, the morphology was never totally lost, even after 60 min of treatment, however, in this case, many cells collapsed (data not shown), Fig. 3C. *E. coli* was exposed to Ag3TNs under dark conditions and as expected, there was little damage; some bacteria increased their sizes and EPS secretions disappeared, but only a few cells showed morphological alterations in their membranes or completely collapsed, Fig. 3D. Some cells exposed to titanate nanotube treatment suffered important damage in the capsule and cytoplasmic membrane.

Control *E. coli* without treatment shows cells with a straight rod shape, a capsule, and a well-defined outer membrane followed by a peptidoglycan layer limited by a cytoplasmic membrane with plenty of ribosomes inside, inclusion bodies and DNA (Fig. 4A); *E. coli* deactivated with silver titanate nanotubes, Ag3NTs: the bacteria increased in size, the central part of the cytoplasm decreased in density, and as can be seen, there is little DNA along the cell (Fig. 4B). Few inclusion bodies underwent reorganization near the cytoplasmic membrane. The capsule lost the rod shape and shows blebs: some parts are totally disrupted. Prior to total damage in the cell, the peptidoglycan layer became anomalously wide. *E. coli* exposed to silver titanate nanotubes without light were less damaged; many cells show normal morphology whereas others were damaged (Fig. 4C); the capsule of the cell lost its

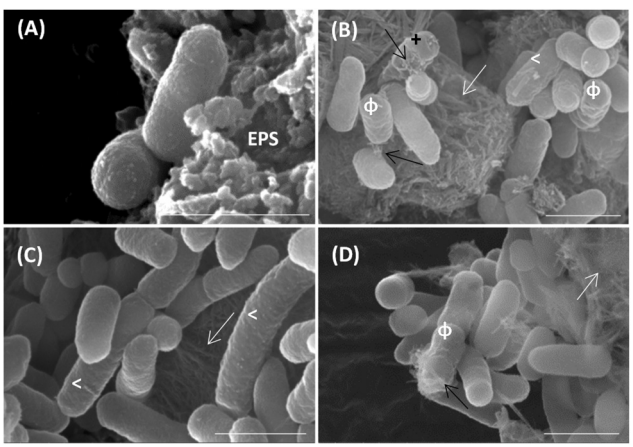

Fig. 3 Morphological evaluation of *E. coli* after 45 min of different treatments (SEM): (A) control, (B) photoactivated silver titanate nanotubes, Ag3NTs, (C) Ag3TNs under dark conditions, and (D) titanate nanotubes alone. EPS, extracellular polymeric substances, +, collapsed cells; the black arrow shows NTs; the white arrow shows aggregates of NT_S; <, elongation size cells; white Φ, capsule damage. In A–D scale bars represent 1 μm.

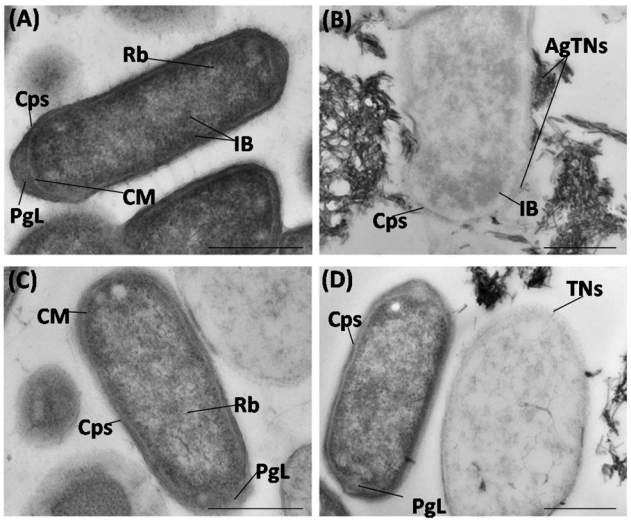

Fig. 4 Morphological evaluation of *E. coli* after 45 min of different treatments (TEM): (A) control, (B) photoactivated silver titanate nanotubes, Ag3TNs, (C) Ag3TNs under dark conditions, and (D) titanate nanotubes alone. Cps, capsule; PgL, proteoglycan layer; CM, cytoplasm membrane; Rb, ribosome; IB, inclusion body; AgTNs, silver titanate nanotubes; TNs, titanate nanotubes. In A–D scale bars represent 0.5 μm.

integrity, and shows an empty cytoplasm like the photoactivated ones (Fig. 4D). In the case of the morphological effect of NTs on *E. coli*, the damage under this condition is similar to the photoactive performance of Ag3TNs; the cytoplasm suffered a reorganization with its center losing almost all ribosomes and DNA, with remains showing up at the periphery of the cytoplasm; some capsules swelled and, in some cases, with more pronounced damage, the frontiers of the cell were lost. The main difference between Ag3TN photoactivation *versus* Ag3TNs under dark conditions or only TN treatment is the number of affected cells. Similar TEM images were reported by Văcăroiu *et al.*,[10] using cultivated *E. coli*, where the investigated films induced modification in the membrane permeability, which promoted cell death in 24 h.

These observations confirm the synergistic effect of silver-titanate composites on *E. coli*: (i) the generation of reactive oxygen species (ROS) by titanate photoactivity properties under irradiation that stresses the bacteria,[21–26] the damage to all the cells was observed by the damage to the membrane, collapsed cells, inhibition of EPS and formation of many aggregates of dead cells, Fig. 3B; (ii) the bacteriostatic effect of AgNPs, highly dispersed on the titanate surface that damaged the integrity of the capsule; the dark conditions caused the elongation of the cell size and density loss in the central part of the cell in some cells, Fig. 4B; (iii) the morphological effect of the sharp TNs on *E. coli*; the damage occurred through cytoplasm reorganization, where the center lost almost all ribosomes and DNA, retaining some dense material at the periphery of the cytoplasm.[27] The sharp morphology of the titanate nanotubes damaged the cell wall, where penetration probably caused more serious damage to the capsule and cytoplasmic membrane, Fig. 4D.

The results observed by Warnes *et al.*[26] about noble metal surface toxicity in *E. coli* involved copper ionic species and the generation of reactive oxygen species, which resulted in immediate cytoplasmic membrane depolarization followed by respiration inhibition, DNA degradation and death.

The Ag1NT composite was identified to be the best catalyst for Eosin Y degradation, Fig. 5A. Ethylene diamine tetraacetic acid (EDTA), *n*-butyl alcohol (nBA), and dimethyl sulphoxide (DMSO) were used as reactive radical scavengers for the determination of the influence of holes, hydroxyl and superoxide radicals, respectively. 1 mM of each scavenger was added separately for each experiment in order to determine which reactive oxygen species is most responsible for the dye photodegradation.[28,29] Among the three scavengers used, addition of EDTA and nBA decreased the visible light photodegradation of Eosin Y from 89 to 80%, as shown in Fig. 5B; the performance of EDTA is more effective at the start of the degradation. This shows that holes are the main responsible reactive radicals followed by hydroxyl.

The presence of low loads of AgNPs on the titanate nanotube surface efficiently prevents the electron–hole recombination, allowing visible light absorption by having Ag^0 and Ag^+ interactions in addition to the bactericidal effect of AgNPs. The photocatalytic synergic behavior of composites can benefit the photocatalytic inactivation of *E. coli* mainly by holes and hydroxyl as major responsible reactive radicals activated by visible light radiation.[30] The surface functionalization of AgNPs may create additional energy levels between the conduc-

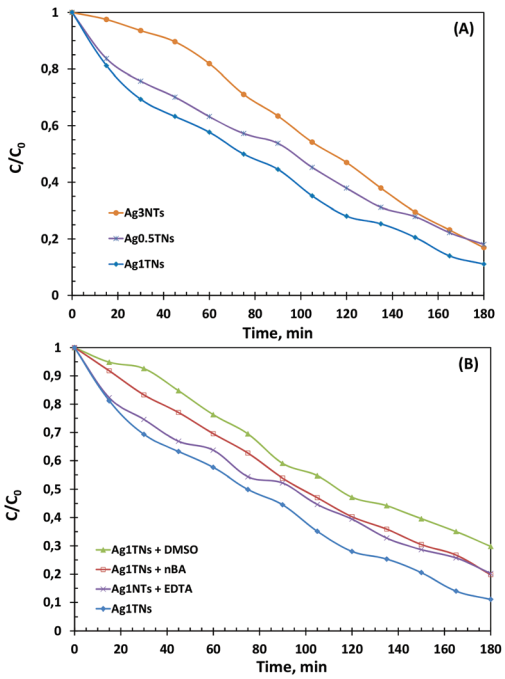

Fig. 5 Photocatalytic degradation of Eosin Y: (A) using AgXNT composites and (B) with the addition of scavenger experiments to identify responsible reactive oxygen species for the photodegradation.

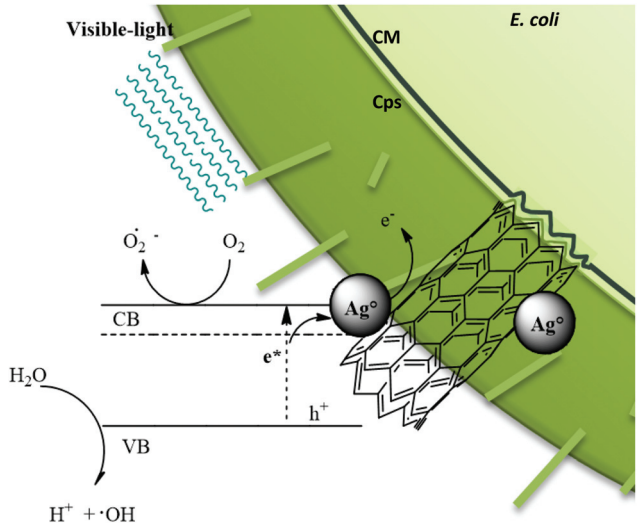

Fig. 6 Schematic representation of the photocatalytic processes that allow the photocatalytic inactivation of *E. coli* by Ag3TNs radiated with visible-light: Cps, capsule; CM, cytoplasmic membrane.

tion band and the valence edge of Ag3TNs that can cause a red-shift in the band edge absorption threshold, Fig. 6.

The synergistic effect of silver titanate nanocomposites caused annihilation of *E. coli* under direct contact with the cell as shown in the TEM images. Ag3TN morphologies caused the death of all cells by damaging the capsule and the cytoplasmic membrane.[14] There is formation of some inclusion bodies near the cytoplasmic membrane and large central area of empty cells. The pathway discovered in this research work is in good agreement with the one previously reported by Saito *et al.*[31] who proposed that a TiO_2 semiconductor caused disorder in cell permeability, achieving the decomposition of the cell wall and cell destruction. Later, Matsugngana *et al.*[32] proposed the oxidation of the intracellular membrane by cell stress respiration that caused the cell death.

The photoactive properties of these nanocomposites promoted by 65 W halogen lamps enhanced enormously the bactericidal and morphological biotoxicity properties of the nanotubes functionalized with AgNPs on the titanate surface.

Conclusions

The practical hydrothermal synthesis of titanate nanotubes and their functionalization with ~5 nm AgNPs allowed the irreversible deactivation of the Gram-negative Enterobacter *E. coli* in a nutritive medium. The high dispersion of AgNPs, mainly in the reduced state (Ag^0) all over the titanate nanotubes, enhanced the charge separation to generate ROS species that stressed the bacteria. The sharp nanotube morphology favored the damage or penetration of the cell, accelerating the fatal inactivation of the *E. coli* under mild conditions, 65 W halogen lamp radiation without using any scavenger.

This practical synthesis of silver nanotube composites has promising green applications that can kill human pathogenic microorganisms with visible light radiation in approximately 45–60 min.

Acknowledgements

We gratefully acknowledge M. C. B. Escoto-Rivera and Dr H. Silva-Pereyra from LINAN-IPICYT for the HRTEM and XRD materials characterization. The authors thank Dr N. A. Ramirez-Pérez and Dr N. Gómez-Hernandez for their technical help during the inactivation experiments. This work was supported by CONACyT projects CB-2011/169597 and LINAN-0271911. R. B. Dominguez-Espíndola and B. P. Nuñez-Luna acknowledge the CONACyT for the granted scholarships.

References

1 J. B. Kaper, J. P. Nataro and H. L. T. Mobley, *Nat. Rev. Microbiol.*, 2004, **2**, 123–140.
2 A. Maule, *J. Appl. Microbiol.*, 2000, **88**, 715–785.
3 E. B. Solomon, S. Yaron and K. R. Matthews, *Appl. Environ. Microbiol.*, 2002, **68**, 397–400.
4 T. Tong, A. Shereet, J. Wu, C. T. T. Binh, J. J. Kelly, J. F. Gaillard and K. A. Gray, *Environ. Sci. Technol.*, 2013, **47**, 12486–12495.
5 S. Amarnath, M. A. Hussain, V. Manjundiah and A. K. Sood, *Soft Nanosci. Lett.*, 2012, **2**, 41–45.
6 N. Musee, M. Thwalaa and N. Nota, *Environ. Monit.*, 2011, **13**, 1164–1183.
7 J. Lee and G. Kaletunc, *Appl. Environ. Microbiol.*, 2002, **68**, 5379–5386.
8 O. Akhavan, M. Abdolahad, Y. Abdi and S. Mohajerzadeh, *J. Mater. Chem.*, 2011, **21**, 387–393.
9 K. Ninomiyaa, M. Arakawab, C. Oginoc and N. Shimizua, *Ultrason. Sonochem.*, 2013, **20**, 762–767.
10 C. Văcăroiu, M. Enache, M. Gartner, G. Popescu, M. Anastasescu, A. Brezeanu, N. Todorova, T. Giannakopoulou, C. Trapalis and L. Dumitru, *World J. Microbiol. Biotechnol.*, 2009, **25**, 27–31.
11 F. Hossain, O. J. Perales-Perez, S. Hwang and F. Román, *Sci. Total Environ.*, 2014, **466–467**, 1047–1059.
12 L. Zhao, H. Wang, K. Huo, L. Cui, W. Zhang, H. Ni, Y. Zhang, Z. Wu and P. K. Chu, *Biomaterials*, 2011, **32**, 5706–5716.
13 V. Rodríguez-González, S. Obregón-Alfaro, L. M. Torres-Martínez, S.-H. Cho and S.-W. Lee, *Appl. Catal., B*, 2010, **98**, 229–234.
14 S. Thabet, F. Simonet, M. Lemaire, C. Guillard and P. Cottona, *Appl. Environ. Microbiol.*, 2014, **80**, 7527–7535.
15 Y. Wang, L. Lin, F. Li, L. Chen, D. Chen, C. Yang and M. Huang, *Photochem. Photobiol. Sci.*, 2016, **15**, 666–672.

16 Y. Zhang, Z. Jiang, J. Huang, L. Y. Lim, W. Li, J. Deng, D. Gong, Y. Tang, Y. Lai and Z. Chen, *RSC Adv.*, 2015, **5**, 79479–79510.
17 N. Liu, X. Chen, J. Zhang and J. W. Schwank, *Catal. Today*, 2014, **225**, 34–51.
18 R. B. Sadu, D. H. Chen, A. S. Kucknoor, Z. Guo and A. J. Gomes, *BioNanoSci.*, 2014, **4**, 136–148.
19 L. Wei, H. Wang, Z. Wanf, M. Yua and S. Chen, *RSC Adv.*, 2015, **5**, 74347–74352.
20 V. Rodríguez-González, S. Obregón-Alfaro, S. M. Lozano-Sánchez and S.-W. Lee, *J. Mol. Catal. A: Chem.*, 2012, **353–354**, 163–170.
21 S. Zhang, C. Liu, X. Liu, H. Zhang, P. Liu, S. Zhang, F. Peng and H. Zhao, *Appl. Microbiol. Biotechnol.*, 2012, **96**, 1201–1207.
22 F. J. Zhang, M. L. Chen and W. C. Oh, *Compos. Sci. Technol.*, 2011, **71**, 658–665.
23 K. Cendrowski, M. Peruzynska, A. Markoeska-Szczupak, X. Chen, A. Wajda, J. Lapczuk, M. Kurzawski, R. J. Kalenczuk, M. Drozdzik and E. Mijowska, *Biomed. Microdevices*, 2014, **16**, 449–458.
24 Q. Kang, Q. Z. Lu, S. H. Liu, L. X. Yang, L. F. Wen, S. L. Luo and Q. Y. Cai, *Biomaterials*, 2010, **31**, 3317–3326.
25 F. Orskov and Orskov, *Methods Microbiol.*, 1984, **14**.
26 S. L. Warnes, V. Caves and W. Keevil, *Environ. Microbiol.*, 2012, **14**, 1730–1743.
27 G. Carréa, E. Hamonc, S. Ennahar, M. Estner, M.-C. Lett, P. Horvatovich, J.-P. Gies, V. Keller, N. Keller and P. Andre, *Appl. Environ. Microbiol.*, 2014, **80**, 2573–2581.
28 N. Krishnarao Eswar, P. C. Ramamurthya and G. Madras, *New J. Chem.*, 2016, **40**, 3464–3475.
29 N. Krishnarao Eswar, P. C. Ramamurthya and G. Madras, *New J. Chem.*, 2015, **39**, 6040–6051.
30 Y. Hou, X. Li, Q. Zhao, G. Chen and C. L. Raston, *Environ. Sci. Technol.*, 2012, **46**, 4042–4050.
31 T. Saito, T. Iwase, J. Hoire and T. Morioka, *Biology*, 1992, **14**, 369–379.
32 T. Matsunaga, R. Tomoda, T. Nakajima and H. Wake, *FEMS Microbiol. Lett.*, 2006, **29**, 211–214.